Stress Perturbations Adjacent to Salt Bodies in the Deepwater Gulf of Mexico

Conference Paper · October 2003

DOI: 10.2118/84554-MS

4 authors, including:

J. T. Fredrich
BP
68 PUBLICATIONS **3,104** CITATIONS
SEE PROFILE

Dave Coblentz
Los Alamos National Laboratory
55 PUBLICATIONS **2,741** CITATIONS
SEE PROFILE

Arlo F. Fossum
None
137 PUBLICATIONS **1,778** CITATIONS
SEE PROFILE

SPE 84554

Stress Perturbations Adjacent to Salt Bodies in the Deepwater Gulf of Mexico

J. T. Fredrich, SPE, D. Coblentz, A. F. Fossum, B. J. Thorne, Sandia National Laboratories

This paper was prepared for presentation at the SPE Annual Technical Conference and Exhibition held in Denver, Colorado, U.S.A., 5 – 8 October 2003.

Abstract

Lack of consideration of the geomechanical interaction between salt bodies and surrounding formations has led to documented drilling failures adjacent to salt diapirs[1-3], in some cases resulting in individual well abandonment costs of tens of millions of dollars. To address this issue, a three-dimensional non-linear finite element geomechanical simulation effort was initiated to analyze the in situ stress state existing in and adjacent to salt bodies before drilling as well as under producing conditions. This work leverages unique expertise in salt mechanics and computational geomechanical modeling. Non-linear finite element geomechanical models were developed for four idealized deepwater Gulf of Mexico geometries including a spherical salt body, a horizontal salt sheet, a columnar salt diapir, and a columnar salt diapir with an overlying tongue. The analyses reveal that at certain locations for specific geometries: shear stresses may be highly amplified; horizontal and vertical stresses may be significantly perturbed from their far-field values; principal stresses may not be vertical and horizontal (i.e., the vertical stress may not be the maximum stress); and anisotropy in the horizontal stresses may be induced. For some geometries, the vertical stress within and adjacent to the salt is not equal to the gravitational load; i.e., a stress-arching effect occurs. Analogously, the assumption that the horizontal stress within a salt body is equal to the lithostatic stress is shown to be incorrect sometimes. The modeling also suggests an alternative explanation for the so-called rubble zones thought to occur beneath and/or adjacent to salt diapirs, in that they may be an intrinsic consequence of the equilibrium stress field needed to satisfy the different stress states that exist within the salt body and in the non-salt surrounding formations. We demonstrate with an example how this work can enable more rigorous planning of well locations and trajectories by providing more accurate estimates of the vertical and horizontal stresses around and within salt bodies for wellbore stability analyses so as to avoid areas of potential geomechanical instability, and to enable accurate fracture gradient prediction while entering, drilling through, and exiting salt bodies.

Introduction

The deepwater Gulf of Mexico (GoM) is the most active deepwater region in the world, currently providing some of the greatest challenges in scope and opportunity for the industry. The region is estimated to contain undiscovered recoverable resources of at least ~13 billion boe, and is known to harbor exceptional reservoirs such as the Thunder Horse discovery at a water depth exceeding 6,000 ft and with estimated recoverable reserves of at least 1 billion boe. However, the complex salt tectonics and the extreme water and reservoir depths necessitate high development costs, and innovative technology is required to bring these fields on stream. Integral to successful economic development is a well service lifetime of 15-30 years.

Many of the significant deepwater GoM objectives are subsalt, with several thousand feet of salt not being uncommon. At the edge of the industry's experience are salt sections of 10,000-ft thickness that overlie targets at depths of 25,000–30,000 ft below mudline.[4, 5] The cost of drilling these deepwater subsalt wells is substantial, and, in some cases, operators have been forced to sidetrack or even abandon wells after experiencing drilling difficulties, with losses running to several tens of millions of dollars.[3] The zone lying immediately below the salt section is notoriously difficult, and there are well known difficulties in accurately predicting fracture gradient and pore pressure immediately upon exiting the salt body.[3-5]

There are necessarily two key components in assuring the considerable investment that must be made to develop these deepwater subsalt fields. First, the planning of well locations and trajectories needs to consider the large-scale geomechanical loading conditions that exist in and around massive salt bodies, and second, the well casing designs need to consider the long-term casing loading that will occur because of salt creep. In this paper we present some of our work addressing the first area that relates to the large-scale geomechanical setting, and specifically, to unique geomechanical effects associated with the presence of massive salt bodies. Our other work that addresses the second component focuses on wellbore-scale finite element modeling to assure the long-term integrity of through-salt well casings and is presented elsewhere.[6, 7]

Constitutive behavior of salt and implications for the local state of stress adjacent to salt bodies

Besides being central to the geologic evolution of important oil and gas provinces such as the Gulf of Mexico, salt bodies affect the present-day geomechanical environment through alteration of the local state of stress.[8] Fundamentally, this is because salt cannot sustain deviatoric stresses, and at mean stresses above roughly 5 MPa (725 psi), deforms via plastic (isovolumetric) creep in response to any imposed deviatoric stress.

In passive sedimentary basins, the state of stress is driven by gravitational loading such that the vertical stress S_V is caused by the weight of the overburden and the horizontal stress S_H is equal to some fraction of the vertical stress S_V.[9] However, this state of stress cannot be sustained within salt bodies, where the stresses relax to an isotropic state of stress with $S_H = S_V$. (Note that we distinguish between isotropic and lithostatic states of stress. A lithostatic state of stress is a special case of an isotropic stress state where both the horizontal and vertical stresses are equal to the gravitational load. Though it is commonly assumed within the industry that the state of stress within salt bodies is lithostatic, the only requirement is in fact for the stress state to be isotropic. We return to this important point later in the paper where we show that the state of stress within a salt body is not lithostatic for some geometries).

The isotropic stress state that exists within the salt body is contrary to the stress state in the surrounding materials that can support a deviatoric stress state with $S_H \neq S_V$. The requirement for the salt body to be in equilibrium and maintain continuity with the surrounding formations therefore causes the stress state near the interface to be highly complex and perturbed from the far-field stress state. The only way to determine the local stress state is to solve the complete set of equilibrium, compatibility, and constitutive equations with the appropriate initial and boundary conditions. The essential purpose of the work described here is to quantify the character and magnitude of these stress perturbations for geometric configurations typical of those found in the deepwater GoM.

Constitutive model for salt

To develop the structural prediction technology to model the complex behavior of natural salt occurring at the Waste Isolation Pilot Plant (WIPP) site, the U.S. Department of Energy's (DOE) repository for transuranic waste generated by U.S. national defense programs, a long-term test program was embarked upon in the late 1970's that included extensive laboratory testing, constitutive model development, and field testing for validation. It was decided at the outset that to develop the requisite predictive capability commensurate with the needs of the U.S. defense programs in a regulatory context, it would be desirable to rely on first principles or, where that was impossible, on laboratory empirical data as the proper basis for the technology. To this end, a constitutive model was developed called the Multimechanism Deformation (MD) model.[10-12] The MD model, which is implemented in finite element codes, is significant because it is based, as much as possible, on first principles (i.e., identified deformation mechanisms), as opposed to a phenomenological model that is based strictly on macroscopic observations. This aspect is important because the former approach is required to extrapolate beyond the conditions used in the laboratory to determine the constitutive parameters of the model. While a phenomenological model may fit experimental data very well, it is not necessarily a good predictor for conditions of pressure, temperature, and time outside those of the laboratory experiments.

Constitutive Equations. The MD constitutive model is formulated by considering individual mechanisms that include dislocation glide, dislocation climb, and a thermally activated but undefined mechanism that is experimentally well characterized.[10] The constitutive equations are formulated on the basis that the total strain rate, $\dot{\varepsilon}_{ij}$, comprises an elastic term, $\dot{\varepsilon}^e_{ij}$, and an inelastic term, $\dot{\varepsilon}^i_{ij}$, according to

$$\dot{\boldsymbol{\varepsilon}}_{ij} = \dot{\boldsymbol{\varepsilon}}^e_{ij} + \dot{\boldsymbol{\varepsilon}}^i_{ij}$$

in which the elastic strain rate is given by the generalized Hooke's law and the inelastic term is intended to treat all aspects of inelasticity. The generalized (three-dimensional) form of the inelastic strain rate is given by

$$\dot{\varepsilon}_{ij} = \frac{\partial \sigma^c_{eq}}{\partial \sigma_{ij}} \dot{\varepsilon}^c_{eq}$$

where σ^c_{eq} and $\dot{\varepsilon}^c_{eq}$ are the power-conjugate equivalent stress and strain rate measures for creep.[12] This generalized flow law is derived based on a thermodynamic formulation in which the power-conjugate equivalent stress measure plays the role of a flow potential and the derivative with respect to stress, σ_{ij}, defines the flow direction.

Inelastic flow caused by dislocation creep is volume preserving and independent of pressure. These features lead to a conjugate equivalent stress measure for dislocation creep, σ^c_{eq}, which is formulated based on the stress difference as given by

$$\sigma^c_{eq} = \left|\sigma_1 - \sigma_3\right|$$

where σ_1 and σ_3 are the maximum and minimum principal stresses, with compression being positive. This stress measure is preferred over that of von Mises because experimental measurements of the flow surface and inelastic strain rate vector are in better agreement with the former formulation.[11]

The kinetic equation representing the creep rate, $\dot{\varepsilon}^c_{eq}$, caused by dislocation flow mechanisms is given by

$$\dot{\varepsilon}^c_{eq} = F \sum_{i=1}^{3} \dot{\varepsilon}_{s_i}$$

where F is a function representing transient creep behavior, and $\dot{\varepsilon}_{s_i}$ is the steady state strain rate for the i^{th} independent dislocation flow mechanism.[10] The mechanisms include dislocation climb ($i = 1$), dislocation glide ($i = 3$), and one that has not been identified mechanistically but which is fully

characterized experimentally (i = 2). The steady state strain rates are

$$\dot{\varepsilon}_{s_i} = A_i e^{-Q_i/RT}\left[\frac{\sigma_{eq}^c}{G}\right]^{n_i}$$

for i = 1 and 2, and

$$\dot{\varepsilon}_{s_i} = H\left(\sum_{i=1}^{2} B_i e^{-Q_i/RT}\right)\sinh\left[\frac{q}{G}\left(\sigma_{eq}^c - \sigma_0\right)\right]$$

for i = 3; where the A_i's and B_i's are constants; Q_i's are activation energies; T is absolute temperature; R is the universal gas constant; G is shear modulus; n_i's are the stress exponents; q is the stress constant; H is the Heaviside function with $\sigma_{eq}^c - \sigma_0$ as the argument; and σ_0 is the stress limit of the dislocation glide mechanism.

The transient function, F, is given by

$$F = \begin{cases} \exp\left[\Delta\left(1-\dfrac{\zeta}{\varepsilon_t^*}\right)^2\right], & \zeta \le \varepsilon_t^* \\ 1, & \zeta = \varepsilon_t^* \\ \exp\left[-\delta\left(1-\dfrac{\zeta}{\varepsilon_t^*}\right)^2\right], & \zeta \ge \varepsilon_t^* \end{cases}$$

which comprises a work-hardening branch, an equilibrium branch, and a recovery branch. The Δ and δ represent the work-hardening and recovery parameters, respectively, and both may be stress dependent; ζ is the hardening variable; and ε_t^* is the transient strain limit. The temperature and stress dependence of the transient strain limit is represented by

$$\varepsilon_t^* = K_0 e^{cT}\left(\frac{\sigma_{eq}^c}{G}\right)^m$$

where K_0, c, and m are constants.[11] The evolution rate, $\dot{\zeta}$, of the isotropic hardening variable ζ is governed by

$$\dot{\zeta} = (F-1)\dot{\varepsilon}_s$$

which approaches zero when the steady-state condition is achieved.

Site Specific Salt Models. Sandia's expertise in modeling salt was further extended through work performed as scientific advisor to the U.S. DOE for the Strategic Petroleum Reserve (SPR), a series of underground storage sites located in salt domes along the U.S. Gulf Coast. In Ref. 8 we show that WIPP salt, although from a bedded formation, can be considered representative of the known deformation behaviors of U.S. Gulf Coast domal salts. Based on validation studies at the WIPP site and on observations of SPR cavern behavior compared with model studies, it was concluded that the current state of the art in salt modeling is adequate to model the deformations and stress fields of underground structural configurations for the ranges of temperature and stresses of interest to WIPP and SPR. Although the conditions expected for deepwater GoM field development are more severe than those encountered at the WIPP or SPR sites, they nonetheless fall within the ranges of stress and temperature for which the mechanistically based salt models have been developed.[8]

Deepwater GoM Salts. Refs. 6-8 present laboratory creep tests performed on rotary sidewall cores taken from a deepwater GoM salt body adjacent to the Mad Dog field. The laboratory tests reveal this deepwater salt to be a relatively "strong" salt, and, moreover, show the creep response of this deepwater GoM salt to be nearly identical to the creep behavior of the Bayou Choctaw Gulf Coast salt. Besides possibly representing the deepest salt cores ever subjected to controlled laboratory creep tests, this work is also significant because it suggests that the known behavior of SPR Gulf Coast salts[13] can be expected to typify the behavior of deepwater GoM salts. Based upon these results, the constitutive parameters for the Bayou Choctaw salt model have been applied in the current work (Table 1).

Three dimensional non-linear geomechanical finite element simulations

The finite element code JAS3D, based on massively parallel distributed memory multiprocessor computers, is ideally suited for large-scale geomechanics analyses. The code utilizes explicit quasi-static solvers developed under DOE Defense Programs to handle very large nuclear-weapons problems with complex material constitutive models and contact surfaces. The use of parallelized iterative solvers and the experience gained with the use of nonlinear material models provide the base technology for efficient solution of large, geometrically complex problems.

JAS3D is capable of predicting the mechanical response of soil and rock over the spatial and temporal scales of interest to the oil and gas industry, including the geologic scale (hundreds to thousands of kilometers and millions of years), reservoir scale (tens of kilometers and tens of years), and wellbore scale (meters and days to years). Through work performed for the U.S. DOE, a library has been developed of constitutive models for geomaterials that are implemented in JAS3D. In addition to the salt model discussed above, Drucker-Prager and Mohr Coulomb models are available, as well as more sophisticated cap plasticity models for describing the deformation of compacting reservoir rocks.[6, 14] Several prior studies demonstrate that JAS3D can handle the mechanics applications that are critically important to the exploration and production activities of the oil and gas industry.[6, 7, 15-17]

Geomechanical models

A suite of approximately twenty-five three-dimensional finite element meshes was developed to represent various subsalt and near-salt geometric configurations typical of the deepwater GoM. The meshes were generated with CUBIT, a two- and three-dimensional finite element mesh generation toolkit.[18] The meshes are graduated to provide increased

resolution close to the salt where the stress changes are greatest, and the number of elements in the models ranges from approximately 10,000 to 20,000. The idealized geometries include a spherical salt body, salt sheet, columnar salt diapir, and columnar salt diapir with tongue. Several permutations were developed for each idealized geometric model to determine the sensitivity of the stress perturbations to various geometric attributes. Figures 1 to 3 show examples of the meshes developed for each of the four idealized geometries, and Figure 4 shows seismic cross sections illustrating salt body geometries observed in the deepwater GoM that served to motivate each model. Geometric and numerical details of the finite element meshes are given in Table 2.

A thorough validation study was performed at the outset to compare the numerical finite element predictions for the pancake geometry model (with elastic material models applied to the pancake and surrounding formations) to the analytic solutions of Geertsma[19] for an elastic disk-shaped (i.e. pancake geometry) reservoir subjected to pore pressure change, with increasingly sophisticated material models also being applied for systematic comparison with the elastic solutions. Note that while a discrete disk-shaped reservoir interval is included in each of the finite element meshes, the work that is described herein only includes the analyses to calculate the initial stresses that exist before drilling and drawdown.

Material Models. The salt creep model is reviewed in an earlier section and is described more completely in Ref. 8. The bulk salt density is prescribed at 2076.5 kg/m^3, which equates to a nearly fully dense salt with ~4% porosity. The surrounding far field is defined as an elastic material, and two sets of simulations were performed with Young's modulus, E, equal to 6 GPa and 12 GPa, with Poisson ratio of 0.225, and a density of 2220 kg/m^3. Most models also contain a reservoir interval that is described with a cap plasticity model; however, since the focus of the current paper does not include the stress evolution that occurs as a consequence of production-induced drawdown we do not describe the reservoir material model in detail here.

Boundary Conditions and Model Extent. The boundary conditions applied to the models for the finite element analyses are the combination of the four vertical faces that are free to displace vertically and in directions parallel to the boundary, but constrained from displacing in directions normal to the boundary, with a bottom surface that is fixed in the vertical direction. The top surface of each model is subjected to a surface load equivalent to a 1219 m (4000 ft) water column. Particular care was taken to locate the lateral boundaries sufficiently far from the salt body so that the behavior at the model edges was identical to the far-field stress configuration (see discussion below). For the salt sphere geometry, we found that the model boundary needed to be at least 10,000 m (32,808 ft) from the salt sphere center, but 20,000 m (65,617 ft) distance from the salt center was required for the salt sheet and diapir models. All models were extended to a depth of at least 20,000 m (65,617 ft); the two thickest salt sheet models were extended to 50,000 m (164,042 ft) depth.

Far-field Conditions. The deepwater GoM is a normal faulting environment, with the maximum principal stress being vertically oriented and the horiziontal stresses equal to some fraction of the vertical stress. There is generally considered to be negligible difference between the minimum and maximum horizontal stresses, S_{Hmin} and S_{Hmax}, respectively. Analyses were performed for three values of the far-field stress state: $S_{Hmin} = S_{Hmax} = 0.7S_V$; $S_{Hmin} = S_{Hmax} = 0.85S_V$; and $S_{Hmin} = S_{Hmax} = S_V$ (i.e., lithostatic). Unless otherwise specifically noted, the discussion and figures below pertain to the results with a far-field stress ratio of 0.7 and E=6 GPa. (The results are qualitatively similar but with reduced magnitude for a stress ratio of 0.85. Obviously, the results for the lithostatic case are trivial; these simulations were largely performed as checks). As noted above, the distance from the sea surface to mudline is equal to 4000 ft (1219 m) for all models. An appropriate geothermal gradient of 0.047572 °F/m is applied with the temperature at mudline equal to 38 °F. A hydrostatic pore pressure gradient of 0.44155 psi/ft (0.02262 MPa/m) is applied from the mudline (where the pore pressure is equal to 1766 psi (12.176 MPa)) to the base of the models. Note that from a practical standpoint, only the salt constitutive model is sensitive to temperature. Likewise, in the geomechanical models considered here, the salt constitutive model is not sensitive to pore pressure because the mean stresses are well over 5 MPa (725 psi).

Initial Stresses. The focus of the modeling effort is to predict the stress state in and adjacent to salt bodies that exists at the current time; that is, before disturbance associated with drilling and/or depletion of the subsalt or near-salt reservoir formations. The stress initialization process consists of several discrete steps. First, for each element in the model, the vertical stress is calculated that is caused by gravitational loading from the material vertically overlying the element in question. This vertical stress is initially assumed to be the maximum principal stress, σ_1. Next, the two principal stresses in the horizontal plane, σ_2 and σ_3, are calculated on an element by element basis from the vertical stress previously calculated based on the prescribed far-field stress ratio as defined above. Following this, the model is released iteratively to adjust the stresses in each finite element so as to achieve equilibrium. For the class of problems considered here, this distills down to the material elements that consist of salt relaxing so as to achieve an isotropic stress state. In effect, this is accomplished by the salt elements transferring loads causing their deviatoric stress onto their neighboring non-salt elements and, in some cases, also readjusting their mean stress. Of course, gravity remains active throughout the entire simulation.

The von Mises stress is a convenient stress indicator as it is an invariant shear stress measure given by:

$$\sigma_{VM} = \sqrt{\{\tfrac{1}{2}\,[(\sigma_1-\sigma_2)^2+(\sigma_2-\sigma_3)^2+(\sigma_1-\sigma_3)^2]\}}$$

Simulations are run for a model duration of 50 years, at which point the von Mises stress in the salt is judged to be sufficiently close to zero (~1 MPa or about 3% of the far-field value). We estimate that the time required for the residual shear stress in the salt to relax identically to zero is on the order of thousands of modeling years and, for the purposes of our effort, consider a residual stress of ~ 1 MPa to be negligible.

It is important to note that while the initial stress field prescribed at time zero is equal to the far-field stress field, at

no subsequent time in the modeling sequence are the stresses at any point in the model, including the boundaries, fixed at a prescribed *a priori* value. Therefore, the attainment of the far-field stress condition at the model boundaries at the end of the simulation (i.e., equilibrium) serves as an essential validation of the simulation.

Robustness of the Numerical Predictions. Several exercises were performed to ensure the robustness of the numerical solutions in regard to the stress initialization procedure. For example, the JAS3D code allows different initial stress states to be specified for different material blocks that are defined within the finite element mesh. Because the model is essentially being driven by the inability of the salt to sustain a deviatoric stress, multiple tests were performed to investigate the sensitivity of the simulations to the stress initialization procedures in the salt elements in particular. Duplicate simulations were performed using two different procedures for setting up the initial stress field in the salt. In one, the procedure for setting up an initial stress field in the salt is as described above, and in another, the salt elements are initially prescribed to have a lithostatic state of stress. In the latter case, the salt elements acquire a large deviatoric stress at the first time step once the model is released, which is then iteratively shed onto the neighboring non-salt elements. At equilibrium, the stress predictions for the models are virtually identical for the two different initialization procedures. The only notable difference between the two is that the (model) time necessary for equilibrium to be achieved is somewhat reduced for the case where the initial stress state defined in the salt elements is lithostatic as compared to the far-field condition.

A second set of tests was performed to investigate the sensitivity of the simulations to the creep model employed, and, in particular, to whether the salt is allowed to relax its stresses by steady state creep alone or whether transient creep was also implemented. The results for the two different cases are virtually identical, and again the only tangible difference relates to the (model) time that is required to reach equilibrium.

A third set of tests was performed to investigate the sensitivity of the numerical predictions to the specific salt consititutive model, e.g., using constitutive parameters for the Bayou Choctaw salt versus the WIPP salt. The stress predictions are not sensitive to the particular values of the salt constitutive parameters that are used, which provides additional validation for the modeling approach. This result differs fundamentally from our wellbore-scale modeling,[6, 7] where predictions depend significantly on the salt constitutive parameters. This is a natural consequence of the reservoir-scale modeling's focus on the equilibrium stress field, as compared to the wellbore-scale modeling that focuses on predicting the casing loading that occurs as salt creeps in response to borehole excavation.

Simulation results

The stress perturbations within and adjacent to salt bodies are driven by the inability of the salt to sustain any stress difference. The loading in the model is caused by a combination of gravitational loading and the ratio of horizontal to vertical stress that describes the far-field state. The predicted stress perturbations vary for the different idealized geometric configurations analyzed. For a single salt body geometry, the magnitude of the predicted stress perturbations increases as the horizontal to vertical stress ratio decreases, and with the size of the salt body. The following sections describe the general characteristics of the stress perturbations for different idealized geometries. The most permutations examined are for the spherical and pancake geometry models and we therefore focus on these two idealized geometries in the following sections. Besides describing the perturbations in the vertical and horizontal stresses, we also describe the variation in the von Mises stress.

Spherical salt body

Three different variations of the salt sphere geometry (Fig. 1) are analyzed corresponding to sphere diameters of 500 m (1640 ft), 1000 m (3281 ft), and 2000 m (6562 ft); unless otherwise indicated, any quoted numerical values refer to the results for the sphere with 2000 m (6562 ft) diameter. As discussed previously, the salt can only sustain an isotropic state of stress. For a spherical geometry with a far-field stress state characterized by $S_H < S_V$, this need to attain an isotropic state of stress drives the vertical stress in the salt down whereas the horizontal stress in the salt is driven up so as to match the vertical stress in the salt (Figure 5).

Because the normal stresses are required to be continuous across the salt – non-salt interface, the changes in the vertical and horizontal stresses that occur within the equilibrated salt sphere necessarily extend into the non-salt formation surrounding the salt sphere. As a result, the vertical stress is decreased both above and below the salt sphere. The horizontal stress is elevated adjacent to the lateral edge of the salt sphere but reduced immediately above and below the salt sphere. These results are more clearly seen in Figure 6 that plots vertical transects through the sphere centerpoint, the outer edge of the sphere (i.e., the first vertical transect that does not intersect salt), and through the far field. Whereas the vertical stress perturbations above and below the salt body extend approximately one-half to three-quarters of a sphere diameter, the horizontal stress perturbations above and below the salt sphere are more spatially restricted, extending less than one-half a sphere diameter above and below the salt body. As a consequence of the perturbations in the local vertical and horizontal stresses, the ratio of horizontal to vertical stress can vary from less than 0.6 to nearly 0.85 at different locations adjacent to the salt body (the ratio is equal to 1 within the salt body itself).

The von Mises stress is obviously negligible within the salt body, but it is profoundly perturbed from the far field in the region surrounding the salt body, with maximum perturbations on order of 50% of the far-field stress (Fig. 6c). The von Mises stress is significantly reduced relative to the far-field value both above and below the salt sphere, but significantly elevated in the material laterally adjacent to the salt sphere (Fig. 5c). The perturbations in the von Mises stress extend approximately one sphere diameter above and below the salt sphere.

Horizontal Stress Anisotropy. A further consequence of the stress changes within and surrounding the salt body is the existence of a horizontal stress difference adjacent to the salt

body (Figure 7) despite the fact that the far-field stress condition is defined with no horizontal stress difference (i.e., $S_{Hmin} = S_{Hmax}$). The magnitude of the stress anisotropy is substantial, with the maximum horizontal stress difference equal to approximately 35% of the far-field horizontal stress. It can be seen by comparison of Figs. 5c and 7 that the spatial locations of maximal horizontal stress anisotropy and von Mises stress coincide.

Rotation of Principal Stresses. The changes in vertical, horizontal, and shear stresses adjacent to the salt body are sufficient to cause re-orientation of the principal stress directions. While it is common practice in the industry to assume that one of the principal stresses is vertically oriented, the principal stress directions are in actuality perturbed in the entire non-salt material immediately outside of the salt body. In localized regions (above and below the salt sphere), the stress rotations can be as high as 15°. Visualization of the three-dimensional principal stress rotations is non-trivial for the complex and dense finite element meshes that are required for the analyses performed here. We present elsewhere a new visualization algorithm that is based on the use of the Mohr's diagram as a tensor glyph for interactive exploration of tensor variables within complex three-dimensional finite element models.[21]

Characteristic Length Scale. As noted above, three separate models are constructed with different sphere sizes (but centered at the same depth) to identify the effect of the salt body size on the magnitude and length scale of the stress perturbations. The results are most easily examined by considering the von Mises stress (Figure 8). Note that this plot corresponds to horizontal transects from the sphere centroid, so that the maximum shear stress amplification in each model is somewhat higher than shown in this plot, because the maximum von Mises stress occurs below the mid-point of the sphere – see Fig. 5. (It is only logical to compare the results along this horizontal transect as only the sphere centroid is at constant depth for all three model permutations.) The amplification in the von Mises stress is a factor of 1.6 for the 2000 m diameter sphere, but reduces to 1.3 for the 500 m diameter sphere. The von Mises stress achieves the far-field value by a distance equal to two sphere diameters (from the sphere centroid) for each of the models.

Effect of Far-field Elastic Properties. Duplicate simulations were performed for several models in which the Young's modulus of the non-salt formations is changed from E=6 GPa to E=12 GPa. The difference between the analyses is negligible; this is interpreted to result from the fact that the stiffness of the salt (E=31 GPa) is substantially greater than the reasonable range in stiffneses of the non-salt formations. As discussed later, application of a non-elastic material model that includes a shear-limit surface (e.g., Mohr Coulomb, Drucker Prager, or cap plasticity) will alter the predicted stress distribution.

Horizontal salt sheet (pancake geometry)

Approximately fifteen permutations of the salt sheet model (Fig. 2) are analyzed to examine the role of salt thickness, distance between the salt sheet and top of the reservoir, and lateral extent of the salt sheet (Table 2). For simplicity, we focus here on the results for the models in which the lateral dimension of the salt sheet (10,000 m or 32,808 ft) is ~ 2× the lateral dimension of the reservoir (5181 m or 17,000 ft). We also focus on the results for the deep salt sheet (top of salt at ~3000 m), as these models are most comparable to the sphere models (salt centroid at 4000 m depth).

Generally, the predicted stress perturbations for the 2000 m thick salt sheet model (Figure 9) are smaller than the stress perturbations predicted for the 2000 m diameter salt sphere (Fig. 6). For the 61, 610, and 2500 m (200, 2000, 8202 ft) thick salt sheets, the vertical stress within the salt body is not perturbed from the lithostatic stress condition. However, the vertical stress is slightly perturbed (increased) from the far-field condition (lithostatic) in the region adjacent to the edge of the salt sheet. Horizontal stress is increased from the far-field value within the salt sheet (where it is equal to the lithostatic stress), but it is markedly reduced from the far-field value both above and below the salt sheet. While the von Mises stress is elevated from the far-field value both above and below the salt sheet, the stress fluctuations are on order of 10-15% of the far-field value for the 2000 m thick salt sheet, as compared to the 2000 m diameter salt sphere where perturbations up to 50% occur. Rather than resulting from significant horizontal stress differences, the zones of elevated von Mises stress above and below the salt sheet result from the reduction in the horizontal stress as compared to the vertical stress. More significantly, note that the sign of the stress perturbation is different for the two geometries: for the spherical geometry, the von Mises stress is reduced (rather than increased) in the overburden and underburden directly above and below the center of the salt sphere. A significant horizontal stress difference exists in the region immediately adjacent to the lateral edge of the salt sheet. For the 610 m (2000 ft) thick salt sheet, the horizontal stress difference is as high as ~25% of the far-field horizontal stress, whereas the horizontal stress difference is up to 35% of the far-field stress for the 2500 and 5000 m (8202 and 16,404 ft) thick salt sheets.

Discussion

While the constitutive behavior of salt is well known, the influence of salt deformation at both the wellbore and reservoir scales is less understood. In particular, lack of consideration of the geomechanical interaction between salt bodies and surrounding formations has sometimes led to drilling failures adjacent to salt diapirs. In the deepwater GoM, the incurred costs can easily reach tens of millions of dollars when an operator is forced to sidetrack or abandon a subsalt or near-salt well.

The large-scale stress perturbations are driven by the necessity of the salt to be encompassed by a material that can sustain the deviatoric stress state that naturally occurs in passive sedimentary basin settings while at the same time to be relaxed to an isotropic stress state. The requirement for the salt body to be in equilibrium and to maintain continuity with the surrounding formations causes the stress state near the interface to be highly complex and perturbed from the far-field stress state. The only way to determine the stress perturbations is to solve the complete set of equilibrium, compatibility, and constitutive equations with the appropriate initial and boundary conditions using a numerical solution technique

such as the finite element method. Nevertheless, certain general observations can be made from the calculations that have been performed here.

The predicted stress perturbations vary for the different idealized geometric configurations analyzed. For the models considered, the magnitude of the predicted stress perturbations increases with the size of the salt body and as the horizontal to vertical stress ratio decreases. The geometry of the salt body has a substantial effect on the qualitative character of the stress perturbations. In general, spheroidal or bulbous salt bodies are predicted to cause more significant stress perturbations than two-dimensional geometries such as salt sheets.

Thin horizontal-lying salt sheets, even if laterally extensive, are not predicted to cause significant stress perturbations, other than directly within the salt body, where the horizontal stress will equal the vertical stress. Substantial stress perturbations are only apparent for salt sheet thicknesses in excess of several thousand feet. Only small vertical stress perturbations are predicted for salt sheets less than 10,000 ft thick, and for these cases, the vertical stress predicted from density logs can be expected to be accurate (an exception being the region laterally adjacent to the edge of the salt sheet, where the vertical stress is distorted from the far field). However, horizontal stress is significantly reduced both above and below salt sheets with thicknesses of several thousand feet, and, correspondingly, the von Mises shear stress is elevated. More significantly, considerable anisotropy in the horizontal stresses occurs in the region immediately adjacent to the edge of the salt sheet.

As the aspect ratio of the salt sheet decreases and approaches a more spheroidal geometry, the characteristics of the stress perturbations evolve towards the behavior seen with the salt sphere models. For an aspect ratio of one (sphere), the isotropic stress in the salt body is between the far-field values of the vertical and horizontal stresses. For aspect ratios greater than 4:1, the isotropic stress in the salt body is equal or very close to the far-field vertical stress.

When the vertical stress is not equal to gravity loading

The case of the spherical salt body is particularly intriguing as the geometry of the salt body in combination with the far-field stress condition causes a re-distribution of stresses such that the vertical stress above, through and below the salt sphere is not equal to the weight of the overlying material. That is, the salt's inability to sustain a stress difference causes some fraction of the weight of the overburden to be borne not by the underlying material, but instead by the laterally adjacent material. Likewise, a similar phenomenon occurs for the salt sheet model with aspect ratio of 2:1 and salt thickness of 5000 m (16,404 ft). (Note that this result is relevant given that at least one operator has recently drilled a 15,000 ft thick salt section.) In other words, a stress-arching phenomenon can naturally exist in the overburden above massive salt bodies before drilling or production. The stress-arching that occurs is similar in character to that which develops in the overburden during production-induced pore pressure drawdown of compactable reservoirs.[6, 15-16]

As shown by comparing Figures 1 and 4, while the salt sphere and salt sheet geometries are idealizations, they nevertheless bear direct relation to actual salt bodies observed in the deepwater GoM. The implications of this result are far reaching in that, to date, the industry has not considered that the vertical stress may not be accurately estimated by integration of density logs. Such vertical stress estimations figure prominently in calculations of mud weight windows necessary to ensure wellbore stability during drilling. The standard assumption that the horizontal stress in a massive salt body equals the lithostatic stress is likewise shown to be potentially faulty, with analogous implications for wellbore stability predictions.

Implications for the origin of rubble zones

The so-called rubble zones that are thought to occur beneath and/or adjacent to some salt bodies have traditionally been interpreted to be 'drag' zones formed as the salt diapir rises through and displaces the overlying and surrounding sediments.[3, 21] Our modeling suggests another plausible explanation for these rubble zones. The formation immediately adjacent to a salt body can experience significantly elevated shear stresses that are simply an intrinsic result of the equilibrium stress field needed to satisfy the different stress states that exist within and outside of the salt body. In some cases, the elevated shear stresses may be sufficient to cause that material to reach shear failure. For example, consider the horizontal stress anisotropy that is predicted to exist at some locations adjacent to salt diapirs and that even at constant mean stress, shear strength decreases as the disparity between σ_2 and σ_3 increases (i.e., the von Mises stress increases).

Clearly, application of a non-elastic material model that includes a failure surface (e.g., Mohr Coulomb or Drucker Prager) has the potential to alter the predicted stress perturbations, in that the maximum allowed stresses in any element will be bounded by the shear-limit surface. While additional simulations can be performed for comparison, the focus of the work reported here has been to identify the nature and potential magnitudes of the stress perturbations that may exist within and adjacent to massive salt bodies in the deepwater GoM.

Impact of stress perturbations, horizontal stress anisotropy, and principal stress rotations on minimum mud weight necessary for wellbore stability

The predicted horizontal and vertical stress perturbations, including introduction of a horizontal stress anisotropy and rotations in the principal stress directions, have important implications for well planning and borehole stability calculations.[22] As an example, we consider the impact of the predicted stress changes adjacent to the 2000 m diameter spherical salt body. The analysis interval is 5609 m (18,400 ft) depth, corresponding to the location where the stress perturbations are greatest. Adjacent to the salt, there is a 10% decrease in the vertical stress as compared to the far field (where the vertical stress is the maximum principal stress), and a 10% increase and 20% decrease in the maximum and minimum horizontal stresses, respectively, as compared to the far field (where $S_{Hmax} = S_{Hmin}$). The rotation in the principal stress directions is ~15° from the vertical and horizontal planes. Stresses and material parameters (typical for shales at

significant depth) are listed in Table 3. Figure 10 shows the required minimum mud weights calculated for acceptable stability for three alternative scenarios as follows: considering the far-field stress condition and ignoring the stress perturbations that exist adjacent to the salt (Fig. 10a); considering the stress perturbations that exist close to salt, but ignoring the rotation in the principal stress directions (Fig. 10b); and considering both the stress perturbations and principal stress rotations that exist close to the salt (Fig. 10c).

In Fig. 10a (representing the far-field stress state), the required minimum mud weight for a vertical well is 82.4 MPa (12.5 ppg), but 89 MPa (13.5 ppg) and 96 MPa (14.6 ppg) for wells deviated at 30° and 60°, respectively (note that the calculations are independent of well azimuth because the far-field condition with $S_{Hmax}=S_{Hmin}$ is assumed). These mud weights provide an acceptable "drilling window" (defined as the difference between the fracture pressure and required mud weight) of at least 10 MPa (1.5 ppg), and drilling problems would therefore not be expected. Note that a GoM rule of thumb is applied in this calculation, whereby the mud pressure that causes circulation losses (i.e., the fracture pressure) is taken as ~1.05× the minimum horizontal stress.

Considering only the perturbation in vertical and horizontal stress magnitudes adjacent to the salt (Fig. 10b), the calculations predict minimum mud weights of 77.8 MPa (11.8 ppg) for a vertical well, 84.5 MPa (12.8 ppg) for a 30° deviated well, and 90.5 MPa (13.7 ppg) for a 60° deviated well. Although there is a difference between the two horizontal stresses, the azimuthal influence on the required mud weight is not significant. However, the lowered minimum horizontal stress adjacent to the salt leads to a ~20% decrease in the fracture pressure – which has a significant consequence on well design. The fracture pressure is estimated at 86.4 MPa (13.1 ppg) for the near-salt reduced minimum horizontal stress of 82.3 MPa. Thus, if a near-salt vertical well is drilled with a mud weight of 82.4 MPa (12.5 ppg) applicable to the far-field stress conditions, circulation losses are possible. Fig. 10b shows that by taking the perturbed stresses into account in the well design, vertical well trajectories are feasible, but with a significantly smaller drilling window. However, stable deviated well profiles greater than 30º are not possible, as the required mud pressures exceed the fracture pressure.

Fig. 10c presents the most rigorous analysis where the principal stress direction rotations are considered – an effect that the industry does not typically consider when performing routine wellbore stability predictions. When the principal stresses are rotated, the directionality implied in the polar plots translates to drilling towards the salt (the "west" direction), away from the salt (the "east" direction) and parallel to the salt (the "north" and "south" directions). The principal stress rotations cause pronounced directionality in the required mud weights and, therefore, preferred drilling directions. The analyses show a minimum mud weight of 80.9 MPa (12.3 ppg) for a vertical well, 83.0 MPa (12.6 ppg) for a well deviated at 30° away from the salt, and 86.0 MPa (13.0 ppg) for a well deviated at 60° away from the salt. These required mud weights increase to 85.9 MPa (13.0 ppg) and 90.3 MPa (13.7 ppg) when drilling towards the salt at 30° and 60° deviation, respectively. Given that the fracture pressure is estimated at 86.4 MPa (13.1 ppg), only well trajectories up to 30° deviation away from the salt are practical. Recognizing this directionality is highly significant for well planning, as wells may be deviated towards a salt body to access formations beneath an overlying tongue, or may exit salt at a high angle to access laterally remote reserves.[23]

The effects of the stress perturbations and rotations on required mud weights are most significant for deviated wells. However, even for drilling a vertical well, where the 82.4 MPa (12.5 ppg) mud pressure calculated for the far-field condition is just within the permissible drilling window, care must still be exercised. Other work[23] has shown that rubble zones that exist around a diapir can suffer time-dependent instability when drilled with a high mud overbalance (i.e., the difference between the mud and pore pressures). Under these conditions, drilling fluid penetration into the surrounding fractured formation is driven by large pressure differentials; the results shown here imply a reduction in the effective overbalance that can lead to irrevocable instability. Thus, even in the case of drilling vertical wells it is essential that required minimum mud weights be reliably predicted so as to avoid excessive overbalance.

Conclusions

1. The large-scale geomechanical interaction between massive salt bodies and the surrounding formations produces conditions that have led to costly drilling failures adjacent to salt diapirs.
2. The isotropic state of stress that exists within salt bodies in the subsurface is at odds with the stress state in the surrounding materials that can support a deviatoric stress state with $S_H \neq S_V$. The requirement for the salt body to be in equilibrium and to maintain continuity with the surrounding formations causes the stress state near the salt interface to be spatially variable and perturbed from the far-field stress state.
3. State of the art three-dimensional nonlinear finite element geomechanical codes that implement sophisticated and validated constitutive models for salt creep can be successfully applied to this problem and used to quantify the character, including magnitude, of stress perturbations within and surrounding salt bodies.
4. Shear stresses adjacent to salt bodies may be highly amplified beyond the far-field value.
5. Vertical stress can be significantly perturbed around (and within) salt bodies so that the vertical stress is not equal to the value that would be calculated by integration of a density log. A stress-arching phenomenon can naturally exist before drilling or production that is similar in character to that which develops in the overburden during depletion of compactable reservoirs.
6. Horizontal stresses may be significantly perturbed from the far-field values in and adjacent to salt bodies. The common assumption that the horizontal stress within a salt body is equal to the lithostatic stress is shown to be incorrect in some cases. For some salt body geometries, anisotropy in the horizontal stresses may be induced which can be as high as 35% of the far-field horizontal stress.
7. Principal stresses may rotate away from the vertical and horizontal planes close to the interface with a salt body,

i.e., the vertical stress may not necessarily be the maximum principal stress. Rotations up to 15° can occur in some locations.

8. The modeling results imply an alternative explanation for the origin of rubble zones that are known to occur beneath or adjacent to some salt bodies. The formation immediately adjacent to a salt body can experience significantly elevated stresses that are an intrinsic consequence of the equilibrium stress field needed to satisfy the different stress states that exist within the salt body and in the far field. In some cases, the elevated shear stresses may be sufficient to cause that material to reach shear failure.
9. Geomechanical modeling of the type employed here enables more rigorous planning of well paths by providing more accurate estimates of vertical and horizontal stresses around and within salt bodies for wellbore stability analyses so as to avoid areas of potential geomechanical instability, and more accurate fracture gradient prediction while entering, drilling through, and exiting salt bodies.

Nomenclature

A_i, B_i = Material constants
E = Young's modulus
F = Transient function
G = Shear modulus
K_0, c, m = Material constants
n_i = Stress exponents
Q_i = Activation energies
q = Stress constant
R = Universal gas constant
S_V = Vertical stress
S_H = Horizontal stress
S_{Hmax} = Maximum horizontal stress
S_{Hmin} = Minimum horizontal stress
α, β = Transient function material constants
Δ = Work hardening parameter
δ = Recovery parameter
ε_t^* = Transient strain limit
σ_1 = Maximum principal stress
σ_2 = Intermediate principal stress
σ_3 = Minimum principal stress
σ_{VM} = von Mises stress
ζ = Internal structure parameter

Acknowledgement

This work was jointly funded by the U.S. Department of Energy's (DOE) Natural Gas and Oil Technology Partnership Program (NGOTP) and by an industry consortium including BHP Billiton, BP, ChevronTexaco, ConocoPhillips, ExxonMobil, Halliburton, Kerr-McGee, and Shell. We are indebted to our industry collaborators, including Lee Chin, Mike Davis, Wolfgang Deeg, Harvey Goodman, Giin-Fa Fuh, Mohamad Khodaverdian, Jim McFadden, Fersheed Mody, Neal Nagel, Dave Olgaard, Ernie Onyia, Steinar Ottesen, Denis Prokofiev, Peng Ray, and Steve Willson for their many insights and contributions to this work, and for their support of the JIP. We especially thank Steve Willson for performing the wellbore stability calculations that are shown in Fig. 10. This work was performed at Sandia National Laboratories funded by the U.S. DOE under Contract No. DE-AC04-AL85000. Sandia is a multiprogram laboratory operated by Sandia Corporation, a Lockheed Martin Company, for the U.S. DOE.

References

1. Bradley, W. B.: "Borehole Failures Near Salt Domes," paper SPE 7503 presented at 1978 Annual Fall Technical Conference and Exhibition, Houston, Oct. 1-3.
2. Seymour, K.P., Rae, G., Peden, J. M., and Ormston, K.: "Drilling Close to Salt Diapirs in the North Sea," paper SPE 26693 presented at the Offshore European Conference, Aberdeen, 7-10 September 1993.
3. Sweatman, R., Faul, R., and Ballew, C.: "New Solutions for Subsalt-Well Lost Circulation and Optimized Primary Cementing," paper SPE 56499 presented at the 1999 SPE Annual Technical Conference and Exhibition, Houston, Oct. 3-6.
4. Rohleder, S. A., Sanders, W. W., Williamson, R. N., Faul, G. L., and Dooley, L. B.: "Challenges of Drilling an Ultra-Deep Well in Deepwater – Spa Prospect," paper SPE/IADC 79810 presented at 2003 SPE/IADC Drilling Conference, Amsterdam, Feb. 19-21.
5. Whitson, C. D., and McFadyen, M. K.: "Lessons Learned in the Planning and Drilling of Deep Subsalt Wells in the Deepwater Gulf of Mexico," paper SPE 71363 presented at 2001 SPE Annual Technical Conference and Exhibition, New Orleans, Sept. 30-Oct. 3.
6. Fredrich, J. T., and Fossum, A. F.: "Large-scale Three-Dimensional Geomechanical Modeling of Reservoirs: Examples from California and the Deepwater Gulf of Mexico," *Oil and Gas Science and Technology – Revue de L'IFP* (2002) **57** 423.
7. Willson, S. M., Fossum, A. F., and Fredrich, J. T.: "Assessment of Salt Loading on Well Casings," *SPEDC* (March 2003) 13.
8. Fossum, A.F., and Fredrich, J.T.: "Salt Mechanics Primer for Near-Salt and Sub-Salt Deepwater Gulf of Mexico Field Developments," Report SAND2002-2063 (2002), Sandia National Laboratories, Albuquerque, New Mexico.
9. McGarr, A., and Gay, N.C.: "State of Stress in the Earth's Crust," Ann. Rev. Earth Planet. Sci. (1978) **6** 405.
10. Munson, D.E., and Dawson, P.R.: "Constitutive Model for the Low Temperature Creep of Salt (with Application to WIPP)", Report SAND79-1853 (1979), Sandia National Laboratories, Albuquerque, New Mexico.
11. Munson, D. E., Fossum, A. F., and Senseny, P.E: "Approach to First Principles Model Prediction of Measured WIPP (Waste Isolation Pilot Plant) In-Situ Room Closure in Salt," *Tunneling and Underground Space Technology* (1990) **5** 135.
12. Fossum, A. F., Callahan, G. D., Van Sambeek, L. L., and Senseny, P.: "How Should One-Dimensional Laboratory Equations be Cast into Three-Dimensional Form?," *Proc. 29th U.S. Rock Mechanics Symp*., A.A. Balkema, Rotterdam (1988) 35.
13. Munson, D. E.: "Multimechanism-Deformation Parameters of Domal Salts Using Transient Creep Analysis," Report SAND99-2104 (1999), Sandia National Laboratories, Albuquerque, New Mexico.
14. Fossum, A. F., and Fredrich, J. T.: "Cap Plasticity Models and Dilatant and Compactive Pre-Failure Deformation," *Proc. 4th North American Rock Mechanics Symp*., A.A. Balkema, Rotterdam (2000) 1169.
15. Fredrich, J. T., Deitrick, G. L., Arguello, J. G., and deRouffignac, E. P.: "Geomechanical Modeling of Reservoir Compaction, Surface Subsidence, and Casing Damage at the Belridge Diatomite Field," *SPEREE* (August 2000) 348.

16. Fredrich, J. T., Holland, J. F., Fossum, A. F., and Bruno, M. S,: "One-Way Coupled Reservoir Geomechanical Modeling of the Lost Hills Oil Field, California," *Proc. 38th U. S. Rock Mechanics Symp*., A.A. Balkema, Rotterdam (2001) 181.
17. Minkoff, S., Stone, C., Bryant, S., Peszynska, M., and Wheeler, M.: "Coupled Fluid Flow and Geomechanical Deformation Modeling," *J. Petr. Sci. Eng*. (2003) **38** 37.
18. Mitchell, S. A., et al.: "CUBIT Mesh Generation Environment Volume 1: Users' Manual," Report SAND94-1100 (2000), Sandia National Laboratories, Albuquerque, New Mexico.
19. Geertsma, J.: "A Basic Theory of Subsidence Due to Reservoir Compaction: The Homogeneous Case," *Verhandelingen Kon. Ned. Geol. Mijnbouwk* (1973) **28** 43.
20. Coblentz, D., Brannon, R. M., Fredrich, J. T., Rogers, D. H., and Crossno, P.: "Imaging Local Stress Perturbations with a Tensor Visualization Algorithm Based on the Mohr Diagram," manuscript submitted to *Geochemistry, Geophysics, Geosystems* (2003).
21. Alsop, G. I., Brown, J. P., Davison, I., and Gibling, M. R.: "The Geometry of Drag Zones Adjacent to Salt Diapirs," *J. Geol. Soc.* (2000) **157** 1019.
22. Willson, S. M., Last, N. C., Zoback, M. D., and Moos, D.: "Drilling in South America: A Wellbore Stability Approach For Complex Geologic Conditions," paper SPE 53940, presented at the 6th LACPEC Conference, Caracas, Venezuela, 21-23 April 1999.
23. Willson, S. M., Edwards, S., Heppard, P. D., Li, X., Coltrin, G., Chester, D. K., Harrison, H. L., and Cocales, B.W.: "Wellbore Stability Challenges in the Deep Water, Gulf of Mexico: Case History Examples from the Pompano Field," paper SPE 84266, presented at the 2003 SPE Annual Technical Conference and Exhibition, Denver, 5 – 8 October 2003.

SI Metric Conversion Factor

feet × 3.048*	E-01	= m
(°F –32)/1.8		= °C
psi × 6.894 757	E-03	= MPa

*Conversion factor is exact.

Table 1. MD Creep Parameters for Bayou Choctaw Salt

Elastic Parameters		Steady State Parameters		Transient Parameters	
G (GPa)	12.4	A_1 (s^{-1})	1.929E22	m	3
E (GPa)	31.0	Q_1 (Kcal/mol)	25	K_0	6.275E5
		n_1	5.5	c, T^{-1}	9.198E-3
		B_1 (s^{-1})	1.400E6	α_w	-13.73
		A_2 (s^{-1})	2.250E12	β_w	-7.738
		Q_2 (Kcal/mol)	10	δ	0.58
		n_2	5.0		
		B_2 (s^{-1})	6.978E-3		
		σ_0 (MPa)	20.57		
		q	5.335E3		
		R (cal/mol-deg)	1.987		

Table 2. Finite Element Meshes and Salt Body Geometries*

Geometry		Description	No. Nodes	No. Elements	Salt Thickness (m)	Salt Depth (m)	Lateral extent (m)
Sphere		Large	9,608	8,136	2,000	5,000 (center)	2,000
		Medium	9,313	7,912	1,000	5,000 (center)	1,000
		Small	7,806	6,576	500	5,000 (center)	500
Sheet	Geometry 2	Thick & Deep	15,933	13,938	610	3,048 (top of salt)	5,182
		Thick & Shallow	12,690	10,998	610	762 (top of salt)	5,182
		Thin & Deep	16,950	14,847	61	3,048 (top of salt)	5,182
		Thin & Shallow	16,950	14,847	61	762 (top of salt)	5,182
Sheet	Geometry 3	Thick & Deep	12,690	10,764	610	3,048 (top of salt)	10,000
		Thick & Shallow	10,764	10,998	610	762 (top of salt)	10,000
		Thin & Deep	10,998	11,466	61	3,048 (top of salt)	10,000
		Thin & Shallow	11,466	11,466	61	762 (top of salt)	10,000
Sheet	Geometry 4	Thicker	49,860	45,672	2,500	3,048 (top of salt)	10,000
Sheet	Geometry 5	Very Thick	38,772	35,033	5,000	3,048 (top of salt)	10,000
Salt Diapir**		No tongue / canopy	12,063	10,128	7010 m	762 (top of salt)	4,266
		With tongue / canopy	7,030	5,544	7010 m	762 (top of salt)	14,630 to 4,266

* Numbers of nodes and elements refer to the quarter-symmetry meshes.
** More complicated meshes were also developed for the two salt diapir geometries that incorporate the basic geometry but without quarter-symmetry.

Table 3. Parameters for Wellbore Stability Analyses

Parameter	Close to Salt	Far Field
Vertical Stress (MPa)	128.8	145.2
Maximum Principal Stress (MPa)	130.2	145.2
Maximum Horizontal Stress (MPa)	113.0	101.6
Intermediate Principal Stress (MPa)	111.7	101.6
Minimum Horizontal Stress (MPa)	82.3	101.6
Minimum Principal Stress (MPa)	82.2	101.6
Estimated Fracture Pressure (MPa)	86.4	106.7
Pore Pressure (MPa)	68.2	68.2
Stress Rotation from Vertical	15.5°	0°
Unconfined Strength (MPa)	25.9	25.9
Friction Angle (degrees)	34°	34°

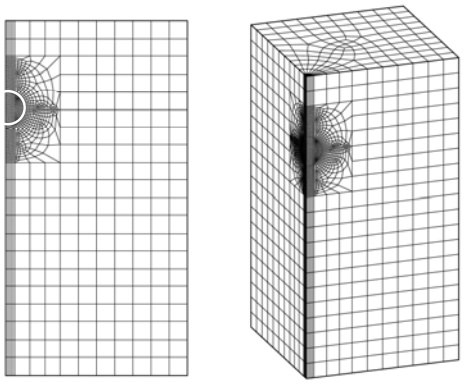

Figure 1. Front (left) and side (right) views of one of the three-dimensional quarter-symmetry finite element meshes developed for the idealized spherical geometry. Similar meshes were developed for two additional sphere sizes. The mesh is extremely dense in the vicinity of the salt sphere, and so the circumference of the salt sphere is overlain on the left view for clarity. See Table 2 for other details of the mesh and geometry.

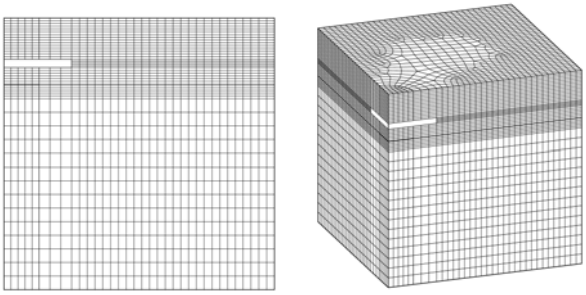

Figure 2. Front (left) and side (right) views of one of the three-dimensional quarter-symmetry finite element meshes developed for the salt sheet geometry. For clarity, the mesh within the horizontal salt sheet is not shown, so that the salt body appears as a solid white block. The reservoir layer is located in the prominent horizontal interval below the salt sheet. In all, about 15 permutations of this idealized geometry were developed to consider different salt sheet thicknesses, distance between the salt sheet and top of the reservoir, and lateral extent of the salt sheet as compared to the underlying reservoir. See Table 2 for other details of the mesh and geometry.

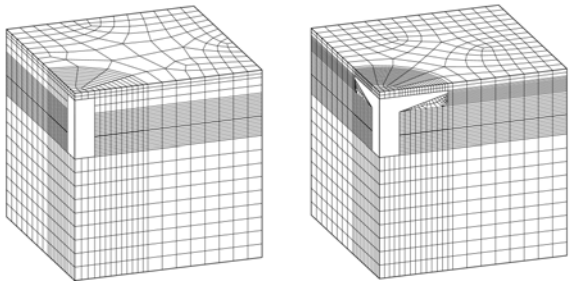

Figure 3. Side views of the three-dimensional quarter-symmetry finite element meshes developed for the columnar salt diapir (left) and columnar salt diapir with tongue (right) geometries. For clarity, the mesh within the salt diapir and tongue are not shown, so that the salt body appears as a solid white block. The reservoir layer is located in the prominent horizontal interval about midway down the salt diapir. Similar three-dimensional meshes were developed for the same geometries that do not have quarter symmetry. See Table 2 for other details of the mesh and geometry.

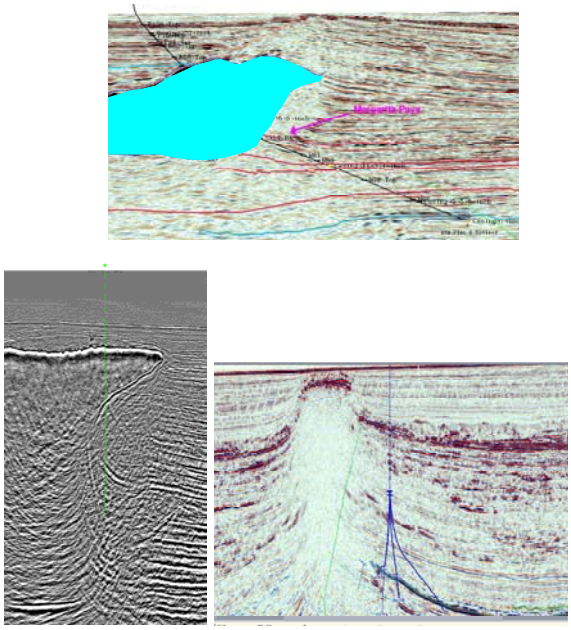

Figure 4. Seismic cross sections showing subsalt and near-salt geometries that are observed in the deepwater GoM and that motivated the idealized geometries studied. The topmost section shows a massive, irregularly-shaped salt body. At different locations, the geometry is not dissimilar from either a spherical body (Fig. 1), or a thick salt sheet (Fig. 2), depending upon the specific location. The section on the lower left motivated the geometry shown in Fig. 3 (right), whereas the section on lower right is similar to that shown in Fig. 3 (left).

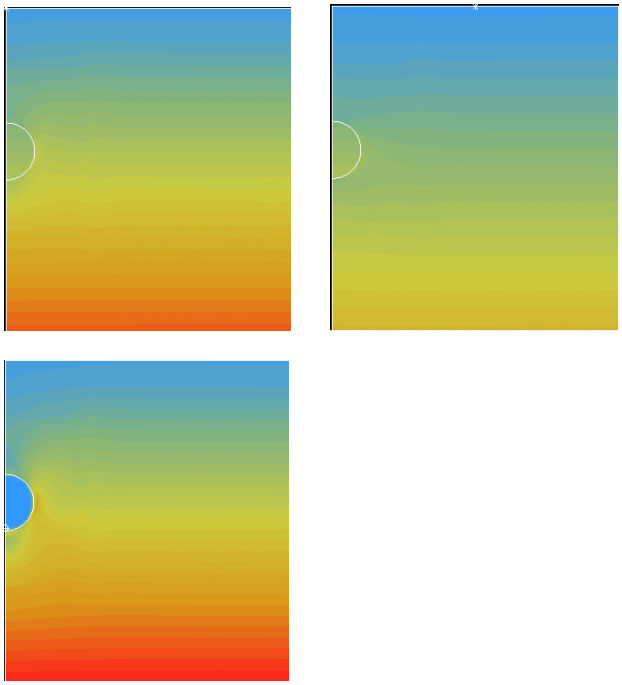

Figure 5. Contour plots of the vertical (top left), horizontal (top right), and von Mises (bottom) stresses for the spherical salt geometry (see the finite element model shown in Fig. 1). The scale bars for the vertical and horizontal stress range from 0 (blue) to 230 MPa (red), and from 0 (blue) to 70 (red) for von Mises stress. Note that the true vertical extent of the model is greater than that shown.

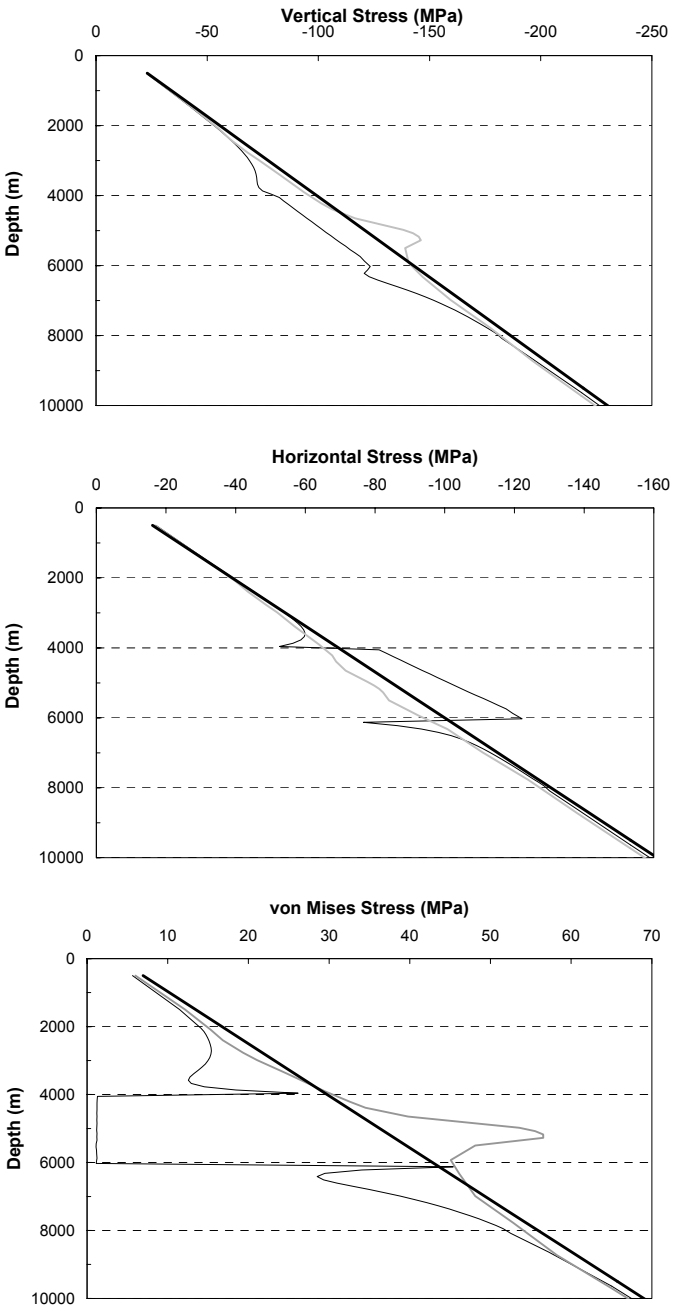

Figure 6. Vertical (top), horizontal (middle), and von Mises (bottom) stresses as a function of depth for a series of vertical transects through the center of the salt sphere, at the outer boundary with the salt sphere, and in the far field. Note that the transects shown do not include the one that traverses the location with maximum von Mises stress. The heavy line is a vertical trajectory through the far field, the thin line is a trajectory through the center of the sphere, and the gray line is a vertical trajectory immediately outside the salt sphere (i.e. outermost material adjacent to the salt body).

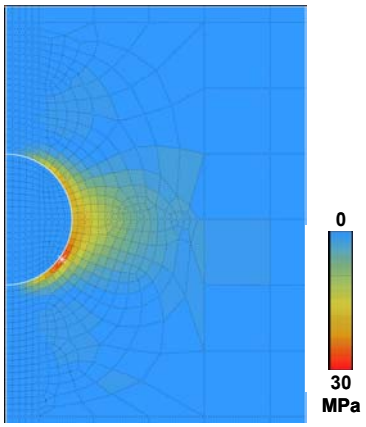

Figure 7. Contour plot showing difference between minimum and maximum horizontal stress for the model shown in Fig. 1. Note that the true vertical extent of the model is greater than that shown.

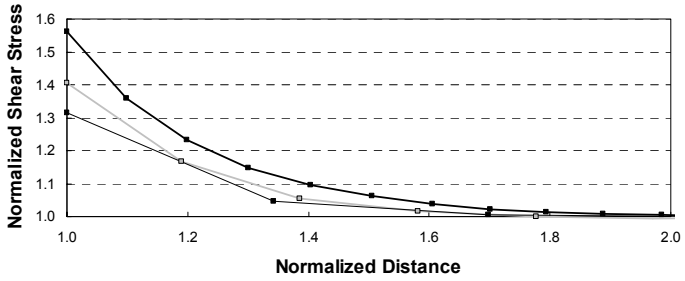

Figure 8. Plot showing von Mises shear stress normalized to the far-field value versus horizontal distance from the salt centroid normalized to the sphere diameter (the edge of the sphere is at x=1.0). For the 2000 m diameter salt sphere (top curve), the normalized stress is identical for far-field stress ratios of 0.7 and 0.85, but the magnitude is slightly reduced for the 1000 m and 500 m spheres for the less deviatoric stress states (middle and bottom curves, respectively). For all three models, the stress state is unperturbed from the far field by two sphere dimensions.

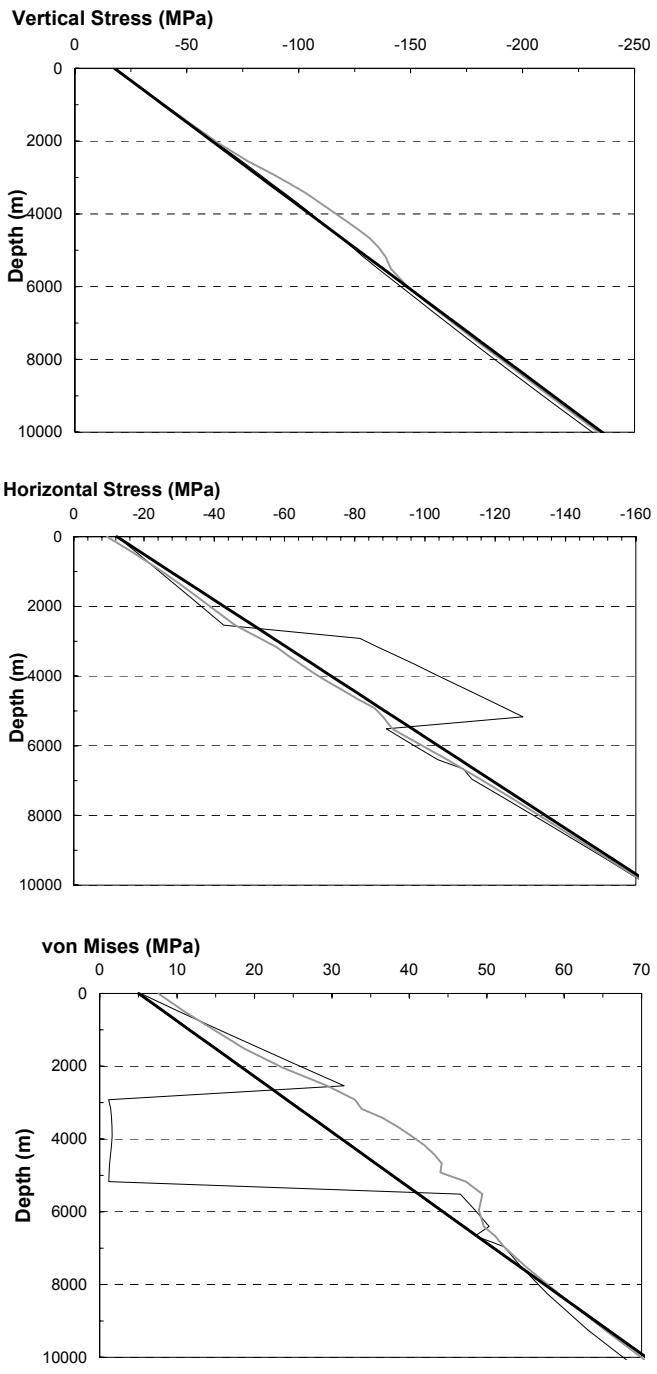

Figure 9. Vertical (top), horizontal (middle), and von Mises (bottom) stresses as a function of depth for a series of vertical transects through the salt sheet model with salt thickness 2500 m (geometry 4 in Table 2). The heavy line is a vertical trajectory through the far field, the thin line is through the center of the salt sheet, and the gray line is a vertical trajectory at the edge of the salt sheet.

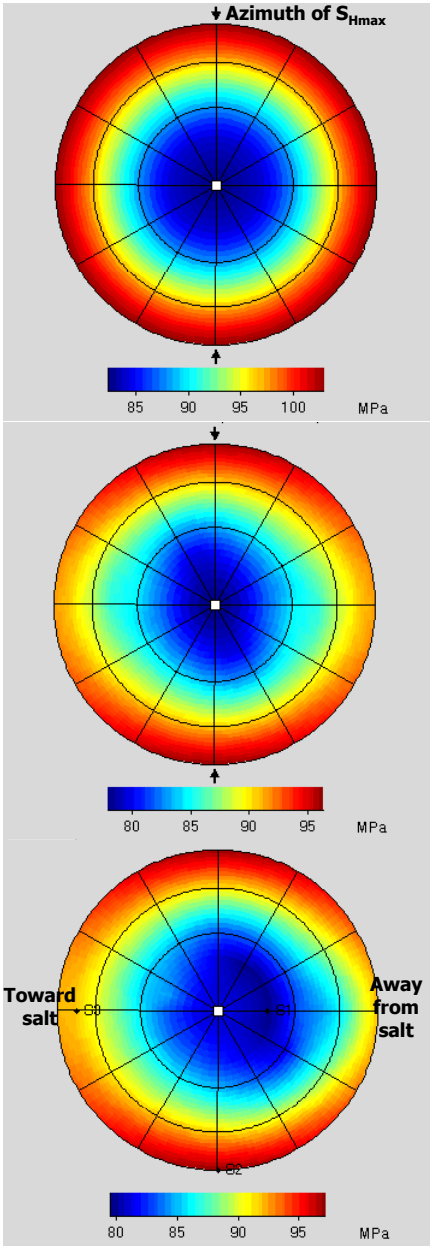

Figure 10. Polar plots of wellbore stability predictions for stress states as detailed in Table 2. The minimum required mud weights for acceptable stability are plotted as a function of wellbore azimuth and inclination. The scale varies for the upper versus lower two plots, and also note the conversions to mud weight that apply for the analysis depth: 80 MPa = 12.1 ppg; 85 MPa = 12.9 ppg; 90 MPa = 13.7 ppg; 95 MPa = 14.4 ppg; 100 MPa = 15.2 ppg. In the plots, a vertical well plots in the center, whereas horizontal wells drilled to the North and East plot at the 12 and 3 o'clock positions on the perimeter, respectively. The interior concentric circles correspond to well deviations of 30° and 60°. The top plot is for the far-field stress state; the predicted minimum mud weights are sufficiently far from the far-field fracture gradient of 106.7 MPa (16.2 ppg) so that deviations up to 60º could be drilled without difficulty. The middle plot is the case where the near-salt vertical and horizontal stress perturbations are considered, but not the principal stress rotation. Only well deviations less than 30º are stable because the near-salt fracture gradient (86.4 MPa = 13.1 ppg) is less than the mud weight required for larger deviations. The lower plot is the case where both the stress perturbations and principal stress rotations are considered. This introduces directionality and only well deviations up to 30º away from the salt are stable.